arXiv:2106.10263v1 [nlin.PS] 18 Jun 2021

Pattern selection in the Schnakenberg equations: From normal to anomalous diffusion

Hatim K. Khudhair[*], Yanzhi Zhang[†], Nobuyuki Fukawa[‡]

Abstract

Pattern formation in the classical and fractional Schnakenberg equations is studied to understand the nonlocal effects of anomalous diffusion. Starting with linear stability analysis, we find that if the activator and inhibitor have the same diffusion power, the Turing instability space depends only on the ratio of diffusion coefficients κ_1/κ_2. However, the smaller diffusive powers might introduce larger unstable wave numbers with wider band, implying that the patterns may be more chaotic in the fractional cases. We then apply a weakly nonlinear analysis to predict the parameter regimes for spot, stripe, and mixed patterns in the Turing space. Our numerical simulations confirm the analytical results and demonstrate the differences of normal and anomalous diffusion on pattern formation. We find that in the presence of superdiffusion the patterns exhibit multiscale structures. The smaller the diffusion powers, the larger the unstable wave numbers and the smaller the pattern scales.

Keywords. Schnakenberg equations, anomalous diffusion, pattern formation, fractional Laplacian, Turing instability

1 Introduction

The reaction-diffusion equations have wide applications in many fields, including biology, chemistry, ecology, geology, physics, finance, and so on. In classical reaction-diffusion equations, the diffusion is described by the standard Laplace operator $\Delta = \partial_{xx} + \partial_{yy} + \partial_{zz}$, characterizing the transport mechanics due to the Brownian motion. Recently, it has been suggested that many complex (e.g., biological and chemical) systems are indeed characterized by the Lévy motion, rather than the Brownian motion; see [5, 6, 12, 17, 18, 27, 28, 30, 33, 40] and references therein. Hence, the fractional reaction-diffusion equations were proposed to model these systems, where the Lévy anomalous diffusion is described by the fractional Laplacian $(-\Delta)^\gamma$. So far, many studies can be found on the fractional reaction-diffusion equations [4, 9, 10, 13]. However, the anomalous diffusion and its interplay with nonlinear reactions on pattern formation and selection have not been well understood yet.

In this paper, we study the pattern formation and selection in the Schnakenberg equation to compare the effects of normal and anomalous diffusion. The Schnakenberg equation is one of the simplest reaction-diffusion systems. It has been applied to study pattern formation in, such

[*]Department of Mathematics and Statistics, Missouri University of Science and Technology, Rolla, MO 65409-0020 (Email: hkkz89@mst.edu)

[†]Department of Mathematics and Statistics, Missouri University of Science and Technology, Rolla, MO 65409-0020 (Email: zhangyanz@mst.edu)

[‡]Department of Business and Information Technology, Missouri University of Science and Technology, Rolla, MO 65409-0020 (Email: fukawan@mst.edu)

as animal skins [1, 2, 32], plant root hair initiation [24], and fluid flows [35]. The Schnakenberg equation was first introduced in [31] to study the limit cycle behavior, i.e., temporal periodic solutions. It describes the following reactions: $A \rightleftharpoons X$, $B \to Y$ and $2X + Y \to 3X$, with X Y, A and B representing different chemicals. In this study, we consider the Schnakenberg equation of the following form:

$$\begin{aligned} \partial_t u(\mathbf{x}, t) &= -\kappa_1(-\Delta)^{\frac{\gamma_1}{2}} u + A - u + u^2 v, \\ \partial_t v(\mathbf{x}, t) &= -\kappa_2(-\Delta)^{\frac{\gamma_2}{2}} v + B - u^2 v, \end{aligned} \tag{1.1}$$

where u and v denote the concentration of chemicals X and Y, respectively, and κ_1, κ_2 are their diffusion coefficients. With a slight abuse of notation, we denote A and B as the concentrations of chemical A and B, respectively. We assume that A and B are in abundance so that A and B are kept constant in the model (1.1). The fractional Laplacian $(-\Delta)^{\frac{\gamma}{2}}$ is defined as

$$(-\Delta)^{\frac{\gamma}{2}} u = \mathcal{F}^{-1}\big[|\mathbf{k}|^{\gamma} \mathcal{F}\big[u\big]\big], \qquad \text{for } \ \gamma > 0,$$

where $\mathcal{F}$ represents the Fourier transform, and $\mathcal{F}^{-1}$ denotes the associated inverse transform. Probabilistically, the fractional Laplacian represents the infinitesimal generator of a symmetric γ-stable Lévy process. In the special case of $\gamma_1 = \gamma_2 = 2$, the system (1.1) reduces to the classical Schnakenberg equation [31]. In this study, we are interested in the diffusion power $\gamma_1, \gamma_2 \in (1, 2]$.

Pattern formation and pattern selection have been one of the most important topics in the study of reaction-diffusion equations. For the classical Schnakenberg equations, many theoretical results have been reported in the literature, including the existence of steady states [22–24], various Turing patterns and their stability [3,14,19,21,25,26,34], and Hopf bifurcation analysis [37,38]. In contrast, the study of the fractional Schnakenberg equation still remains scant. In [15], a finite difference method is proposed to solve the variable-order fractional Schnakenberg equations. Recently, there is growing interest in the fractional reaction-diffusion equations (see [4, 8, 9, 13, 29, 39] and reference therein), but the understanding of anomalous diffusion in pattern formation and selection still remains limited. To the best of our knowledge, no report on pattern formations in the fractional Schnakenberg equation can be found in the literature. Moreover, even though there are many theoretic studies on the classical Schnakenberg equation, few numerical studies can be found on pattern formations.

In this work, we analytically and numerically study pattern formation and selection in both classical and fractional Schnakenberg equations. As one of the simplest reaction-diffusion systems, the study of pattern formations in the Schnakenberg equation provides insights to understand anomalous diffusion in reaction-diffusion models and advances their practical applications. We find that the necessary condition for Turing instabilities is $\kappa_1 < \kappa_2$. If $\gamma_1 = \gamma_2$, the fractional Schnakenberg equations have the same Turing spaces as its classical counterpart, but the Turing space increases with the ratio κ_1/κ_2 or γ_1/γ_2. The smaller the power γ_1, the larger the unstable wave numbers and the smaller the pattern scales. Our weakly nonlinear analysis predicts the parameter regimes for hexagon patterns, stripe patterns, and their mixtures. Our numerical results confirmed the theoretical analysis and also provided new insights on the patterns in the fractional Schnakenberg equations. This paper is organized as follows. In Sect. 2, we carry out a linear stability analysis to study Turing instability. In Sect. 3, weakly nonlinear stability analysis and amplitude equation analysis are presented to study the patterns of hexagons, stripes, and their coexistence. Numerical studies of patterns in the classical Schnakenberg equation are presented in Sect. 4, while Sect. 5 is devoted to patterns in the fractional cases. Finally, some conclusions are made in Section 6.

2 Linear stability analysis

In this section, we perform the linear stability analysis for the Schnakenberg model (1.1) and study the conditions for Hopf and Turing bifurcations. For notational convenience, we let $\mathbf{u} = (u, v)^T$ and denote $a = B - A$ and $b = B + A$; thus the system (1.1) can be reformulated as:

$$\begin{aligned} \partial_t u(\mathbf{x}, t) &= -\kappa_1(-\Delta)^{\frac{\gamma_1}{2}} u - u + u^2 v + \frac{b-a}{2}, \\ \partial_t v(\mathbf{x}, t) &= -\kappa_2(-\Delta)^{\frac{\gamma_2}{2}} v - u^2 v + \frac{b+a}{2}. \end{aligned} \tag{2.1}$$

Noticing that $A, B > 0$, we have $b > 0$ and $a \in (-b, b)$ in (2.1). In the absence of diffusion (i.e., $\kappa_1 = \kappa_2 = 0$), the system (2.1) has a unique stationary state $\mathbf{u}_s \equiv \big(b,\ (a+b)/2b^2\big)^T$. Furthermore, the Jacobian matrix of system (2.1) at $\mathbf{u}_s$ is given by

$$J|_{\mathbf{u}=\mathbf{u}_s} = \begin{pmatrix} a/b & b^2 \\ -\big(1 + a/b\big) & -b^2 \end{pmatrix}.$$

It is evident that the steady state $\mathbf{u}_s$ is stable, if the trace and determinant of J satisfy

$$\mathrm{tr}(J) = \frac{a}{b} - b^2 < 0, \qquad \det(J) = b^2 > 0,$$

equivalently, we require $a < b^3$.

Next, we carry out linear stability analysis to understand the stability of $\mathbf{u}_s$ in the presence of diffusion (i.e., $\kappa_1, \kappa_2 \neq 0$). Consider a small perturbation of the steady state $\mathbf{u}_s$, i.e.,

$$\mathbf{u} = \mathbf{u}_s + \boldsymbol{\varepsilon} \exp(\lambda t + i\mathbf{k} \cdot \mathbf{x}), \tag{2.2}$$

where $\boldsymbol{\varepsilon} = (\varepsilon_1, \varepsilon_2)^T$ with $|\varepsilon_1|, |\varepsilon_2| \ll 1$ being the amplitudes of perturbations, $i = \sqrt{-1}$ is the imaginary unit, λ is the growth rate of the perturbation in time t, and $\mathbf{k}$ is the wave vector. Substituting (2.2) into (2.1) and linearizing the system, we obtain

$$\begin{pmatrix} \lambda + \kappa_1|\mathbf{k}|^{\gamma_1} - a/b & -b^2 \\ 1 + a/b & \lambda + \kappa_2|\mathbf{k}|^{\gamma_2} + b^2 \end{pmatrix} \begin{pmatrix} \varepsilon_1 \\ \varepsilon_2 \end{pmatrix} = \begin{pmatrix} 0 \\ 0 \end{pmatrix}.$$

Hence, the characteristic equation of the above system is

$$\lambda^2 - \Big(\frac{a}{b} - b^2 - \kappa_1|\mathbf{k}|^{\gamma_1} - \kappa_2|\mathbf{k}|^{\gamma_2}\Big)\lambda + \Big[\Big(\kappa_1|\mathbf{k}|^{\gamma_1} - \frac{a}{b}\Big)\Big(\kappa_2|\mathbf{k}|^{\gamma_2} + b^2\Big) + b^2\Big(1 + \frac{a}{b}\Big)\Big] = 0. \tag{2.3}$$

The Hopf bifurcation occurs when $|\mathbf{k}| = \mathbf{0}$ and $\mathrm{Re}(\lambda) = 0$, but $\mathrm{Im}(\lambda) \neq 0$. Thus, the boundary of Hopf bifurcation is given by

$$a = b^3.$$

If $\mathrm{Re}(\lambda(\mathbf{k})) > 0$, the unstable wave number $\mathbf{k}$ will grow exponentially until the nonlinearity bounds this growth. The onset of the instability occurs at $\lambda(\mathbf{k}) = 0$, i.e., when

$$\Big(\kappa_1|\mathbf{k}|^{\gamma_1} - \frac{a}{b}\Big)\Big(\kappa_2|\mathbf{k}|^{\gamma_2} + b^2\Big) + b^2\Big(1 + \frac{a}{b}\Big) = 0,$$

which admits the single minimum $(k_{\mathrm{cr}},\, a_{\mathrm{cr}})$:

$$a_{\mathrm{cr}} = \frac{\kappa_1\sqrt{\kappa_1\kappa_2\sigma}\big(\kappa_1\vartheta + \sigma + 1\big)}{\big[\kappa_1\vartheta(1-\sigma) + 1\big]^{3/2}}\,\vartheta^{\frac{3}{2} + \frac{1}{2\sigma}}, \qquad k_{\mathrm{cr}} = |\mathbf{k}_{\mathrm{cr}}| = \vartheta^{\frac{1}{\gamma_1}}. \tag{2.4}$$

Here, we denote $\sigma = \gamma_1/\gamma_2$, implying that $\sigma \in (\frac{1}{2}, 2)$ as $\gamma_1, \gamma_2 \in (1, 2]$. We define ϑ implicitly as:

$$\frac{\kappa_1\kappa_2\,\sigma\,\vartheta^{1+1/\sigma}}{\kappa_1(1-\sigma)\vartheta + 1} = b^2,$$

which implies that $\vartheta > 0$ for $\sigma \in (\frac{1}{2}, 1]$, or $0 < \vartheta < 1/\kappa_1(\sigma - 1)$ for $\sigma \in (1, 2)$. In the special case of $\gamma := \gamma_1 = \gamma_2$, we have $\sigma = 1$ and $\vartheta = b/\sqrt{\kappa_1\kappa_2}$, and thus the critical values in (2.4) reduce to

$$a_{\rm cr} = b^2 r(br + 2), \qquad k_{\rm cr} = \left(\frac{b}{\sqrt{\kappa_1\kappa_2}}\right)^{1/\gamma}, \tag{2.5}$$

where we denote $r = \sqrt{\kappa_1/\kappa_2}$, i.e., the square root of the diffusion coefficient ratio.

From the above discussion and noticing $a \in (-b, b)$, we see that the conditions for the Turing instability (also known as diffusion-driven instability) are given by

$$a_{\rm cr} < a < \min\{b, b^3\}, \tag{2.6}$$

which is referred to as the Turing space. The conditions (2.4)–(2.6) suggest that the Turing space generally depends on the diffusion coefficients κ_1 and κ_2, and the ratio σ of diffusion powers. Particularly, if $\gamma_1 = \gamma_2$ this dependence reduces to the ratio of diffusion coefficients (i.e., κ_1/κ_2), rather than the values of κ_1 and κ_2. Comparing (2.5) and (2.6) suggests that for $\gamma_1 = \gamma_2$, the necessary condition of Turing instability is $\kappa_1 < \kappa_2$, i.e., the inhibitor v should diffuse faster.

Figure 1 illustrates the Turing spaces for different parameters. In Fig. 1(a), we fix the diffusion coefficients κ_1 and κ_2, and compare the Turing spaces for different ratios σ of diffusive powers. It shows that with the increase of σ, the Turing space reduces quickly. Fig. 1(b) shows the effects

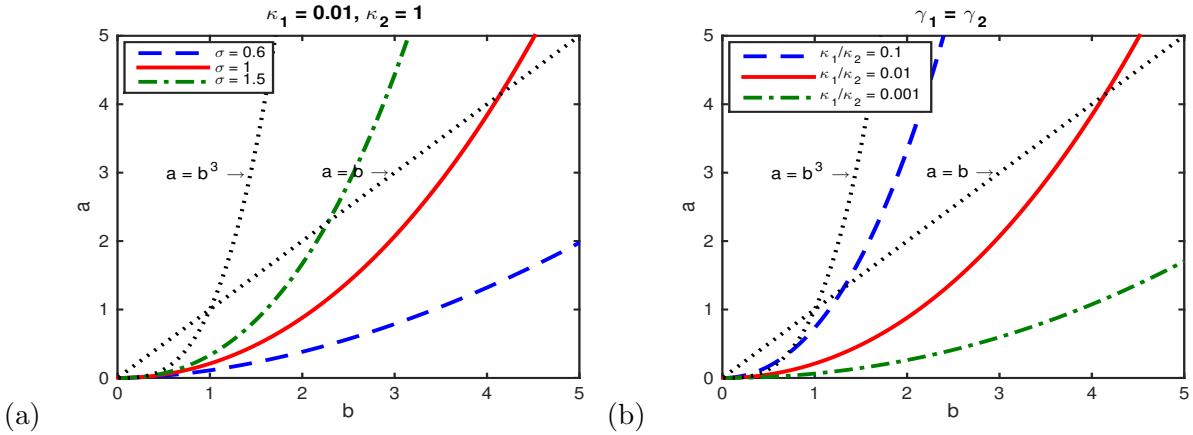

Figure 1: Illustration of Turing spaces (i.e., region between the non-dotted line and dotted-line of $\min\{b, b^3\}$) for different ratios of diffusion powers $\sigma = \gamma_1/\gamma_2$ (a) and coefficients κ_1/κ_2 (b).

of diffusion coefficients for $\gamma_1 = \gamma_2$. We find that the smaller the ratio κ_1/κ_2, the larger the Turing space, and our extensive studies show that this observation is independent of σ. In the special case of $\gamma_1 = \gamma_2$, to ensure the existence of Turing space, the diffusion ratio r should satisfy $r \le \left(-1 + \min\left\{\sqrt{2}, \sqrt{1+b^2}\right\}\right)/b$, which implies that the maximum ratio allowed depends on parameter b.

Figure 2 compares the unstable bands of wave number $k = |\mathbf{k}|$ for different diffusive parameters. Fig. 2(a)–(c) show that for given κ_1 and κ_2, the ratio σ of diffusion powers play an important role in determining the maximum growth rate (i.e., $\max_k \mathrm{Re}(\lambda)$) of the unstable wave number. The

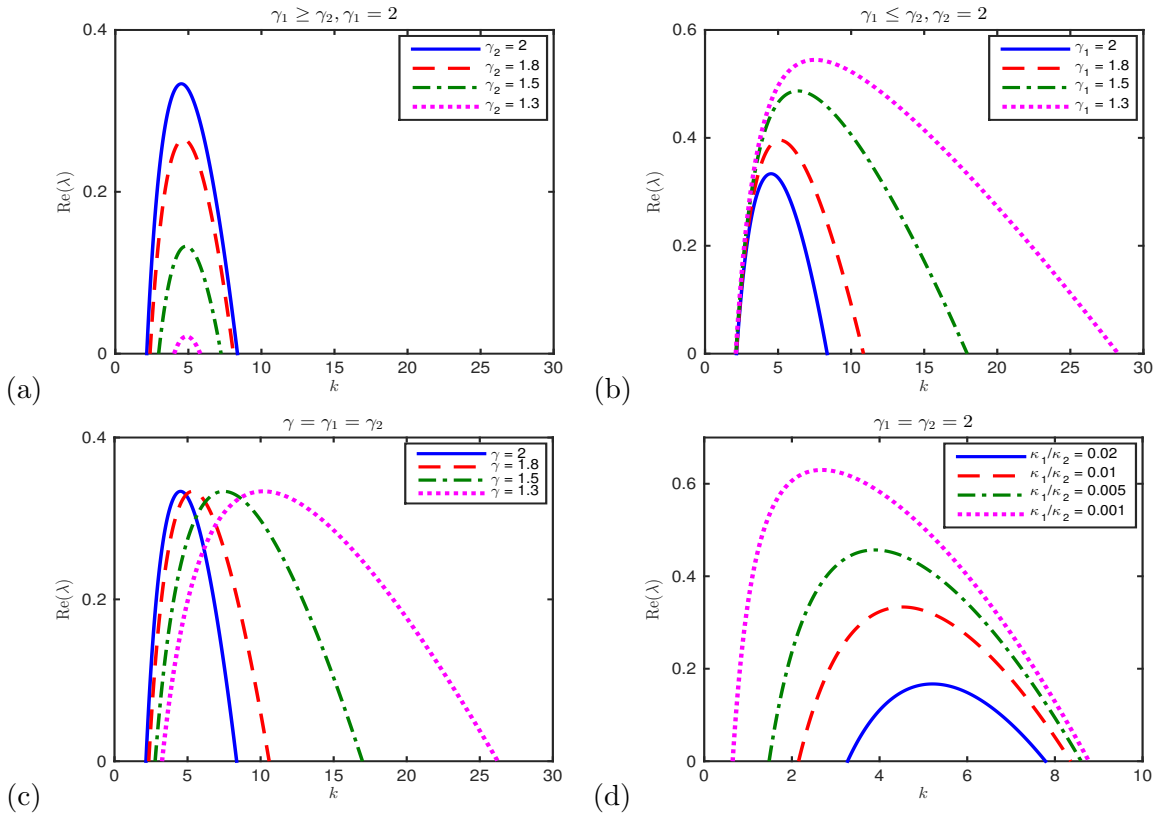

Figure 2: Illustration of growth rates for different parameters, where $a = 1.4$ and $b = 1.8$ are fixed. The diffusion coefficients $\kappa_1 = 0.01$ and $\kappa_2 = 1$ for (a) $\gamma_1 \geq \gamma_2$; (b) $\gamma_1 \leq \gamma_2$; (c) $\gamma_1 = \gamma_2$.

maximum growth rate decreases with increasing ratio $\sigma = \gamma_1/\gamma_2$, and thus maximum growth rates for both classical and fractional cases remain the same as long as $\gamma_1 = \gamma_2$; see Fig. 2(c). It further suggests that the Turing instability could occur even if $\gamma_1 \geq \gamma_2$, but not for $\kappa_1 \geq \kappa_2$. On the other hand, the width of unstable bands depends on the powers γ_1 and γ_2, rather than their ratio. Fig. 2 (c) shows that if $\gamma_1 = \gamma_2$, the fractional Schnakenberg equation has more unstable wave numbers than its classical counterpart. Moreover, the instability tends to occur at larger wave numbers. Fig. 2 (d) additionally compares the unstable wave numbers for different diffusion ratio κ_1/κ_2, where $\gamma_1 = \gamma_2 = 2$. It shows that the decrease of diffusion ratio κ_1/κ_2 broadens the unstable band and also increases the maximum growth rate. Even though decreasing the ratio κ_1/κ_2 or the fractional power γ both lead to a wider unstable band, they are essentially different diffusion mechanics (cf. Fig. 2 (c) & (d)).

3 Weakly nonlinear analysis

The linear stability analysis predicts unstable wave numbers in the system, but it fails to provide insights on the nonlinear coupling of these unstable wave numbers. In the study of pattern formation, however, the nonlinear terms dominate the growth of the unstable modes. In this section, we will perform a weakly nonlinear analysis of the system (2.1) near the Turing instability threshold

$(k_{\rm cr},\, a_{\rm cr})$, where the solution of (2.1) can be written in the form

$$\mathbf{u} = \mathbf{u}_s + \sum_{1\le j\le 3} \Big(\mathbf{A}_j(t)\, e^{i\mathbf{k}_j\cdot\mathbf{x}} + \bar{\mathbf{A}}_j(t)\, e^{-i\mathbf{k}_j\cdot\mathbf{x}} \Big) \tag{3.1}$$

where $\mathbf{A}_j = \big(A_{j,u}, A_{j,v}\big)^T$ denotes the amplitude associated with wave number $\mathbf{k}_j$, and $\bar{\mathbf{A}}_j$ represents its complex conjugate. The wave number satisfies $\mathbf{k}_j = k_{\rm cr}(\cos(2j\pi/3),\, \sin(2j\pi/3))^T$ (for $1 \le j \le 3$), and thus $\mathbf{k}_1 + \mathbf{k}_2 + \mathbf{k}_3 = \mathbf{0}$. In the following, we will denote $e_j = e^{i\mathbf{k}_j\cdot\mathbf{x}}$ for notational simplicity, and will focus on the analysis of $\gamma_1 = \gamma_2 = \gamma$.

Next, we derive the amplitude equations for $\mathbf{A}_j$. Introducing the slow time $\tau = \varepsilon^2 t$, we then expand $\mathbf{u} - \mathbf{u}_s$ and the bifurcation parameter a as:

$$\mathbf{u} - \mathbf{u}_s = \varepsilon\mathbf{u}_1 + \varepsilon^2\mathbf{u}_2 + \varepsilon^3\mathbf{u}_3 + \mathcal{O}(\varepsilon^4), \qquad a = a_{\rm cr} + \varepsilon^2\hat{a} + \mathcal{O}(\varepsilon^3), \tag{3.2}$$

where $\mathbf{u}_i := \mathbf{u}_i(\mathbf{x},\tau) = (u_i, v_i)^T$ for $i = 1, 2, 3$. Substituting (3.2) into (2.1), and collecting like powers of ε, we obtain the sequence of equations as

$$\mathcal{O}(\varepsilon): \qquad \mathcal{L}\mathbf{u}_1 = \mathbf{0}, \tag{3.3}$$

$$\mathcal{O}(\varepsilon^2): \qquad \mathcal{L}\mathbf{u}_2 = \mathbf{c}\bigg(2bu_1v_1 + \frac{1}{2b}\Big(1 + \frac{a_{\rm cr}}{b}\Big)\, u_1^2 \bigg), \tag{3.4}$$

$$\mathcal{O}(\varepsilon^3): \qquad \mathcal{L}\mathbf{u}_3 = \partial_\tau\mathbf{u}_1 + \mathbf{c}\bigg(u_1^2v_1 + 2b(u_1v_2 + u_2v_1) + \frac{1}{b}\Big(1 + \frac{a_{\rm cr}}{b}\Big)\, u_1u_2 + \frac{\hat{a}}{b}u_1 \bigg), \tag{3.5}$$

where the vector $\mathbf{c} = (-1, 1)^T$, and $\mathcal{L}$ denotes the linear operator of the system at the Turing instability threshold, i.e.,

$$\mathcal{L} = \begin{pmatrix} -\kappa_1(-\Delta)^{\frac{\gamma}{2}} + \dfrac{a_{\rm cr}}{b} & b^2 \\ -\Big(1 + \dfrac{a_{\rm cr}}{b}\Big) & -\kappa_2(-\Delta)^{\frac{\gamma}{2}} - b^2 \end{pmatrix}.$$

At $\mathcal{O}(\varepsilon)$, we seek the solution of (3.3) of the form:

$$\mathbf{u}_1 = \begin{pmatrix} \hat{u}_1 \\ \hat{v}_1 \end{pmatrix} \sum_{1\le j\le 3} \Big(W_j(\tau)\, e_j + \bar{W}_j(\tau)\, \bar{e}_j \Big), \tag{3.6}$$

where W_j denotes the amplitude of the wave number $\mathbf{k}_j$ at the first order perturbation (i.e., at $\mathcal{O}(\varepsilon)$). Substituting (3.6) into (3.3) and noticing the values of $a_{\rm cr}$ and $k_{\rm cr}$ in (2.5), we obtain

$$\hat{u}_1 = b, \qquad \hat{v}_1 = -r(br + 1). \tag{3.7}$$

At $\mathcal{O}(\varepsilon^2)$, we can rewrite (3.4) as:

$$\mathcal{L}\mathbf{u}_2 = \mathbf{c}\,\xi\,\big(\Theta + \bar{\Theta}\big)^2 = \mathbf{c}\,\xi \sum_{1\le j\le 4} \big(\Theta_j + \bar{\Theta}_j\big), \tag{3.8}$$

by taking (3.6) and (3.7) into account, where we denote

$$\xi = \frac{b}{2} - b^2 r\Big(1 + \frac{3}{2}br\Big), \qquad \Theta = \sum_{1\le j\le 3} W_j e_j, \qquad \Theta_1 = |\mathbf{W}|^2 := \sum_{1\le j\le 3} |W_j|^2,$$

$$\Theta_2 = \sum_{1\le j\le 3} W_j^2\, e_j^2, \qquad \Theta_3 = 2 \sum_{\substack{j=1,2 \\ j<l\le 3}} W_j\bar{W}_l\, e_j\bar{e}_l, \qquad \Theta_4 = 2\big(W_1W_2\,\bar{e}_3 + W_1W_3\,\bar{e}_2 + W_2W_3\,\bar{e}_1\big).$$

The Θ_4 terms are introduced by the resonant interactions between models e_j, which are usually considered to be small [13]. Hence, we will neglect the terms of Θ_4 in the following discussion. Solving (3.8) gives the solution $\mathbf{u}_2$ as

$$\mathbf{u}_2 = \xi\Big[\begin{pmatrix}\hat{u}_{21}\\ \hat{v}_{21}\end{pmatrix}(\Theta_1+\bar{\Theta}_1) + \begin{pmatrix}\hat{u}_{22}\\ \hat{v}_{22}\end{pmatrix}(\Theta_2+\bar{\Theta}_2) + \begin{pmatrix}\hat{u}_{23}\\ \hat{v}_{23}\end{pmatrix}(\Theta_3+\bar{\Theta}_3)\Big], \tag{3.9}$$

where we define $z_2 = 2^\gamma$ and $z_3 = (\sqrt{3})^\gamma$, and then

$$\begin{pmatrix}\hat{u}_{21}\\ \hat{v}_{21}\end{pmatrix} = -\frac{1}{b^2}\begin{pmatrix}0\\ 1\end{pmatrix}; \qquad \begin{pmatrix}\hat{u}_{2j}\\ \hat{v}_{2j}\end{pmatrix} = -\frac{1}{b^2 r(z_j-1)^2}\begin{pmatrix}-z_j b\\ z_j b r^2 + r\end{pmatrix}, \quad j=2,3.$$

At $\mathcal{O}(\varepsilon^3)$, substituting (3.6) and (3.9) into (3.5), we get

$$\mathcal{L}\mathbf{u}_3 = \partial_\tau \mathbf{u}_1 + \mathbf{c}\big(\Theta+\bar{\Theta}\big)\Big(\frac{\hat{a}}{b}\hat{u}_1 + \sum_{1\le j\le 3}\eta_j\big(\Theta_j+\bar{\Theta}_j\big)\Big), \tag{3.10}$$

where the coefficient η_j is computed by

$$\eta_j = \hat{u}_1^2\hat{v}_1 + 2b\xi\big(\hat{v}_1\hat{u}_{2j} + \hat{u}_1\hat{v}_{2j}\big) + \xi\Big(\frac{1}{b} + br^2 + 2r\Big)\hat{u}_1\hat{u}_{2j}, \quad 1\le j\le 3.$$

By simple calculation, we obtain that

$$\begin{aligned}
\big(\Theta+\bar{\Theta}\big)\big(\Theta_1+\bar{\Theta}_1\big) &= 2\,|\mathbf{W}|^2\sum_{1\le j\le 3}\big(W_j\,e_j + \bar{W}_j\,\bar{e}_j\big),\\
\big(\Theta+\bar{\Theta}\big)\big(\Theta_2+\bar{\Theta}_2\big) &= \sum_{1\le j\le 3}|W_j|^2\big(W_j\,e_j + \bar{W}_j\,\bar{e}_j\big) + \mathcal{T}_2\\
\big(\Theta+\bar{\Theta}\big)\big(\Theta_3+\bar{\Theta}_3\big) &= 2\sum_{1\le j\le 3}\big(|\mathbf{W}|^2 - |W_j|^2\big)\big(W_j\,e_j + \bar{W}_j\,\bar{e}_j\big) + \mathcal{T}_3,
\end{aligned}$$

where we have used the relation $\mathbf{k}_1+\mathbf{k}_2+\mathbf{k}_3 = 0$. The terms $\mathcal{T}_l$ (for $l=2,3$) are the residual terms, which can be ignored in deriving the amplitude equations. Substituting the above results into (3.10) and neglecting residual terms $\mathcal{T}_l$ yields

$$\mathcal{L}\mathbf{u}_3 = \partial_\tau\mathbf{u}_1 + \mathbf{c}\sum_{\substack{1\le j,k,l\le 3\\ j\ne k,l}}\Big(\big(2\eta_1+\eta_2\big)|W_j|^2 + 2\big(\eta_1+\eta_3\big)\big(|W_l|^2+|W_k|^2\big) + \frac{\hat{a}}{b}\hat{u}_1\Big)\big(W_j\,e_j + \bar{W}_j\,\bar{e}_j\big) \tag{3.11}$$

For a linear system $\mathcal{L}\mathbf{v} = \mathbf{r}$, the Fredholm solvability condition suggests that the existence of a nontrivial solution is ensured if the right-hand vector $\mathbf{r}$ is orthogonal to the zero eigenvectors of the adjoint operator $\mathcal{L}^\star$. Here, we have the zero eigenvector of $\mathcal{L}^\star$ as:

$$u^\star = \Big(\frac{1+br}{br}, \quad 1\Big)^T\bar{e}_j, \qquad j=1,2,3. \tag{3.12}$$

Combining (3.4) and (3.5) to obtain a system of $\mathcal{L}\big(\varepsilon^2\mathbf{u}_2 + \varepsilon^3\mathbf{u}_3\big)$, we then apply the Fredholm solvability condition to its right hand side and get

$$\varepsilon b(1-r^2)(br+1)\partial_\tau W_j = 2\xi\bar{W}_k\bar{W}_l + \varepsilon\left[\big(2\eta_1+\eta_2\big)|W_j|^2 + 2\big(\eta_1+\eta_3\big)\big(|W_l|^2+|W_k|^2\big) + \hat{a}\right]W_j \tag{3.13}$$

for permutations of $j,k,l = 1,2,3$.

For notational simplicity, we denote $A_j(t) := A_{j,u}(t)$ for $j = 1, 2, 3$. Then equations (3.1), (3.2) and (3.6) indicate the relation:

$$A_j(t) = \varepsilon \hat{u}_1 W_j(\tau) + \mathcal{O}(\varepsilon^2), \quad j = 1, 2, 3; \qquad \tau = \varepsilon^2 t; \qquad \varepsilon^2 \hat{a} = a - a_{\rm cr}.$$

Here, we will only focus on the amplitude equations for u-component, as $A_{j,v} = \hat{v}_1 A_{j,u}/\hat{u}_1$. Substituting the above relation into (3.13) and reorganizing the terms yields the amplitude equations:

$$c_0 \partial_t A_j(t) = c_1(a - a_{\rm cr})A_j + c_2 \bar{A}_k \bar{A}_l + \Big(c_3|A_j|^2 + c_4\big(|A_k|^2 + |A_l|^2\big)\Big)A_j, \tag{3.14}$$

for the permutations of $j, k, l = 1, 2, 3$, where the coefficients:

$$c_0 = b^3(1 - r^2)(br + 1), \quad c_1 = b^2, \quad c_2 = 2b\xi, \quad c_3 = 2\eta_1 + \eta_2, \quad c_4 = 2(\eta_1 + \eta_3).$$

To study pattern selections, we will carry out the linear stability analysis on the amplitude equations (3.14). Rewrite the amplitude function $A_j = \rho_j(t)\, e^{i\varphi_j(t)}$ (for $j = 1, 2, 3$). Substituting it into (3.14) leads to the systems for density ρ_j and phase $\varphi = \varphi_1 + \varphi_2 + \varphi_3$ as:

$$\begin{aligned} c_0 \partial_t \rho_j(t) &= c_1(a - a_{\rm cr})\rho_j + c_2 \rho_k \rho_l \cos(\varphi) + \big(c_3 \rho_j^2 + c_4(\rho_k^2 + \rho_l^2)\big)\rho_j, \\ c_0 \partial_t \varphi(t) &= -c_2 \, \frac{\rho_1^2\rho_2^2 + \rho_1^2\rho_3^2 + \rho_2^2\rho_3^2}{\rho_1\rho_2\rho_3} \sin(\varphi), \end{aligned} \tag{3.15}$$

for the permutation of $j, k, l = 1, 2, 3$. The density $\rho_1 = \rho_2 = \rho_3 = 0$ for a spatial homogeneous steady state, while for stripe patterns $\rho_1 \neq 0$ and $\rho_2 = \rho_3 = 0$. For the hexagon (or spot) patterns, the density $\rho_1 = \rho_2 = \rho_3 \neq 0$ and phase $\varphi = 0$ or π. Furthermore, the hexagon patterns with $\varphi = 0$ and π are referred to as positive (denoted as H_0) and negative (denoted as H_π) hexagons, respectively. In the following, we will study the parameter regimes of stripe and spot patterns and their stability.

3.1 Stripe patterns

In the case of steady stripe patterns, the density function ρ_j reduces to

$$\rho_1^s = \sqrt{-\frac{c_1(a - a_{\rm cr})}{c_3}}, \qquad \rho_2^s = \rho_3^s \equiv 0. \tag{3.16}$$

It implies that the stripe pattern exists when $c_3 < 0$, since $c_1 > 0$ and $a - a_{cr} > 0$. To understand the stability of stripe patterns, we perform the linear stability analysis on the system (3.15) around the steady state (3.16). For brevity, we omit the detailed calculations. Here, we obtain the characteristic equation:

$$\big[c_1(a - a_{\rm cr}) + 3c_3\big(\rho_1^s\big)^2 - c_0\lambda\big]\big[\big(c_1(a - a_{\rm cr}) + c_4\big(\rho_1^s\big)^2 - c_0\lambda\big)^2 - c_2^2\big(\rho_1^s\big)^2\big] = 0.$$

Substituting the value of ρ_{1s} in (3.16), we obtain:

$$\lambda_1 = -\frac{2c_1(a - a_{\rm cr})}{c_0}, \qquad \lambda_{2,3} = -\frac{c_1(a - a_{\rm cr})}{c_0 c_3}\Big(c_4 - c_3 \pm |c_2|\sqrt{\frac{c_3}{-c_1(a - a_{\rm cr})}}\Big). \tag{3.17}$$

It is evident that λ_1 is always negative. Note that $c_3 < 0$ to ensure the existence of stripes. To ensure the existence of steady stripes, we require that $\mathrm{Re}(\lambda_j) < 0$ for $j = 2, 3$, which is true if the following conditions are satisfied:

$$c_4 < c_3 < 0, \qquad c_1 > -\frac{c_3 c_2^2}{(c_3 - c_4)^2(a - a_{\rm cr})}.$$

3.2 Hexagon patterns

If steady hexagon (or spot) patterns exist, their densities satisfy

$$\rho_1 = \rho_2 = \rho_3 = \rho_h, \tag{3.18}$$

where ρ_h is defined implicitly by

$$(c_3 + 2c_4)\rho_h^2 + |c_2|\rho_h + c_1\big(a - a_{\rm cr}\big) = 0. \tag{3.19}$$

It immediately implies that the positive density $\rho_h > 0$ exists only when $c_3 + 2c_4 < 0$. Then using the linear stability analysis and equation (3.19), we obtain the growth rate of perturbations as

$$\lambda_1 = -\frac{1}{c_0}\big[2c_1(a - a_{\rm cr}) + |c_2|\rho_h\big], \qquad \lambda_{2,3} = \frac{2}{c_0}\big[\big(c_3 - c_4\big)\rho_h - |c_2|\big]\rho_h.$$

If $\rho_h > 0$ exists, there is always $\lambda_1 < 0$, and thus the spot pattens are stable if $(c_3 - c_4)\rho_h < |c_2|$. Summarizing the above discussion, we obtain the conditions for stable spot patterns as

$$c_3 + 2c_4 < 0, \qquad (c_3 - c_4)\rho_h < |c_2|.$$

Furthermore, if $c_2 > 0$ (resp. < 0) the patterns are H_0 (resp. H_π) hexagons.

Figure 3 illustrates the parameter regimes of steady stripe and hexagon patterns in the Turing space of classical Schnakenberg equations. It shows that H_0 and H_π hexagon patterns exist at the two ends of the Turing space, while stripe patterns are found between these two regions. The

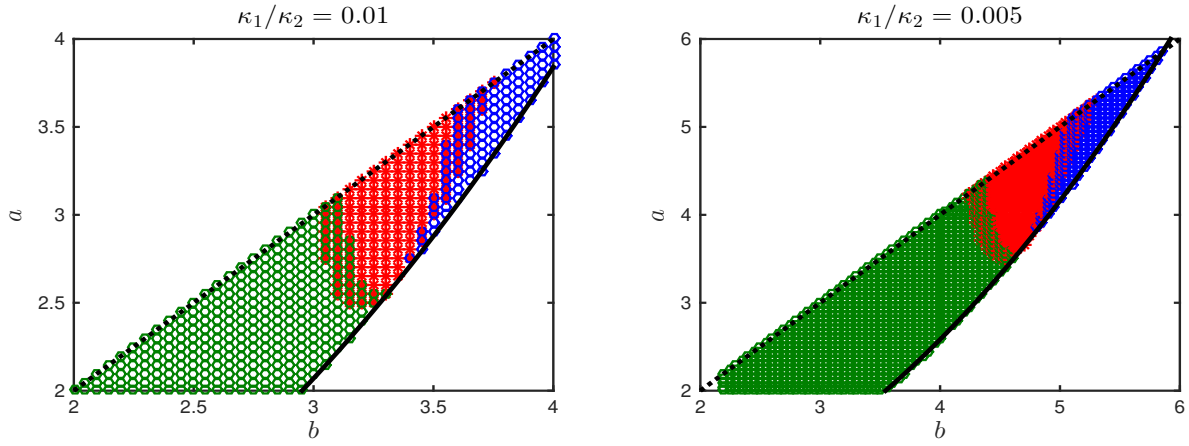

Figure 3: Illustration of stripe (red asterisk), H_0 hexagon (green circle), and H_π hexagon (blue circle) in the Turing space for different diffusion ratios, where $\gamma_1 = \gamma_2 = 2$.

overlap of stripe and spot regions are observed, where the stability conditions for both stripes and spots are satisfied. Hence, the mixed patterns of spots and stripes occur in the overlapping regions. We find that even though the diffusion ratio affects the Turing space, the distribution regions of steady patterns are qualitatively the same. Additionally, the parameter regions for classical and fractional cases with $\gamma_1 = \gamma_2$ are almost the same, although their amplitude equations (3.14) are different (because c_3 and c_4 depend on γ).

Our weakly nonlinear analysis predicts the parameter regimes for different patterns. In Section 4 and 5, we will perform numerical simulations to study pattern formation in both classical and fractional Schnakenberg equations and compare them with our theoretical predictions. To this end,

the two-dimensional Schnakenberg equation (2.1) with periodic boundary condition is discretized by the Fourier pseudospectral method in space and 4th order Runge–Kutta method in time. In our simulations, we will choose the domain $\Omega = [-4, 4]^2$ with number of grid points $N_x = N_y = 1024$ and time step $\Delta t = 0.005$. The initial condition is taken as the steady states $\mathbf{u}_s$ with a small perturbation on $[-0.01, 0.01]^2$. We have refined the mesh size and time step to make sure the conclusions are independent of these numerical parameters. In all pattern plots, only patterns of u_1 are presented, where red and blue represent the highest and lowest values of u_1, respectively. Unless otherwise stated, we will always choose $\kappa_2 = 1$ in the following simulations.

4 Pattern formation with normal diffusion

So far, pattern formations in the Schnakenberg equation have not been well understood, even in the classical (i.e., $\gamma_1 = \gamma_2 = 2$) cases. Studies on some special parameters are reported in the literature [16, 36], but no exhaustive report can be found on pattern formation and selection across different parameter regimes. To study the normal and anomalous diffusive effects, we will thus start with patterns in the classical Schnakenberg equation with different regimes of parameters a, b, and $r = \sqrt{\kappa_1/\kappa_2}$. Our extensive simulations show that patterns exist only when $a \geq a_{\rm cr}$, confirming the analytical results in Sec. 2. In particular, steady patterns at $a = a_{\rm cr}$ could vary greatly for different values of b.

Figure 4 illustrates for representative patterns in the Turing space of the classical Schnakenberg equation with $\kappa_1 = 0.01$, where we could divide the Turing space into two regimes. In Regime I but $a \gg a_{\rm cr}$, only spot patterns are observed (i.e., pattern (a) in Fig. 4). By contrast, patterns in Regime II are more complicated. Various patterns, including stripes, spots, and mixture of stripes

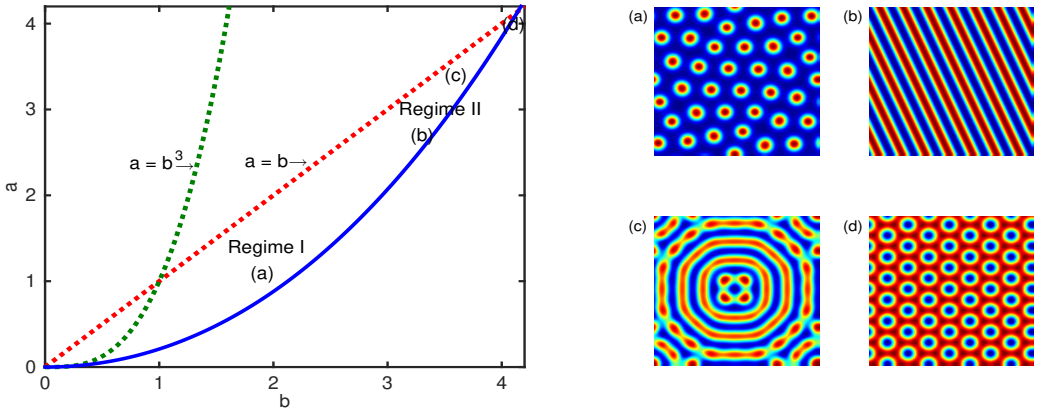

Figure 4: Illustration of pattens in the classical Schnakenberg equation with $\kappa_1 = 0.01$.

and spots, are observed (see pattern (b)-(d) in Fig. 4), depending on the combination of a, b and r. Hexagon patterns are observed in both Regime I and II, which are H_0 hexagons in Regime I and H_π hexagons in Regime II (cf. patterns (a) and (d) in Fig. 4). These numerical observations confirm our weakly nonlinear analysis predictions in Fig. 3.

Figure 5 further demonstrates the patterns and corresponding dispersion relation for various b and $a \in (a_{\rm cr}, b]$, where $\kappa_1 = 0.01$. For $b = 1$, the weakly nonlinear analysis shows that only spot patterns exist for any a, which is confirmed by our numerical results in Fig. 5. It shows that the patterns are qualitatively the same, but the larger the value of a, the denser the spots. For different a, the dispersion relation reaches its maximum at the same wave number, but the growth

rate and unstable band increase with a. We additionally find that in Regime I, the density of spots

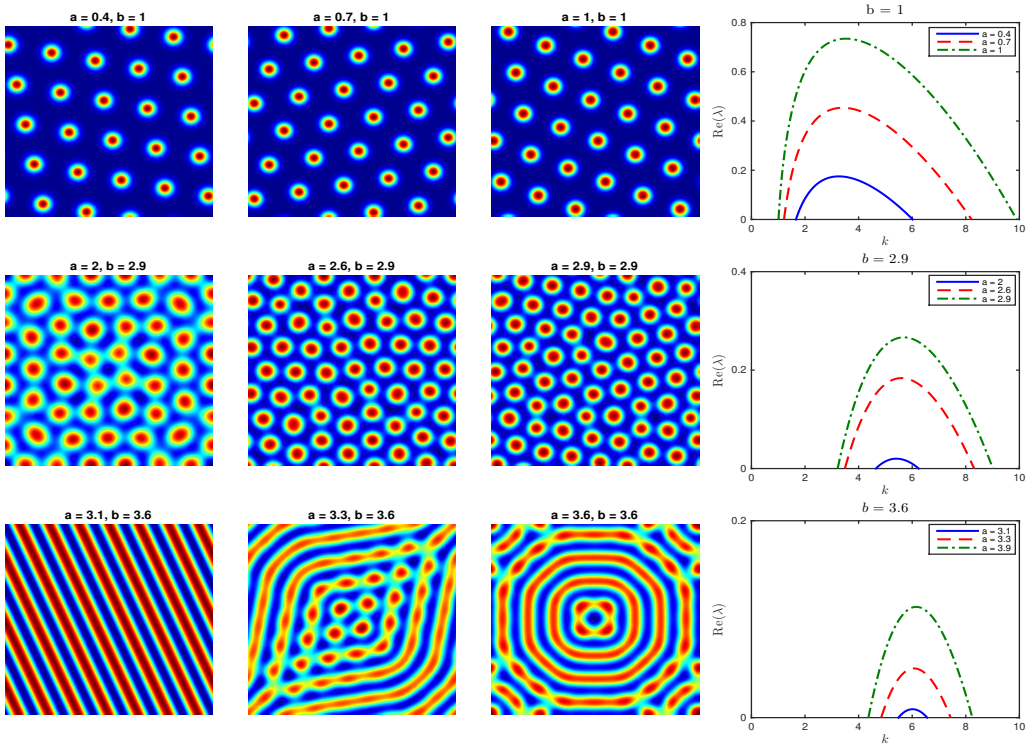

Figure 5: Patterns and dispersion relation in the classical Schnakenberg equation with $\kappa_1 = 0.01$.

in the steady patterns generally increases with the value of b. Different from $b = 1$, spots start to connect when $b = 2.9$, locating in transition regime between I and II. The patterns for $b = 3.6$ are more complex, depending on the value of a. Stripe patterns are observed for a slightly larger than $a_{\rm cr} = 3.0586$ (see Fig. 5 with $a = 3.1$). As a increases, the stripes start to deform, and spots appear in the pattern, resulting in a mixed pattern of spots and stripes. It also shows that the growth rate in this case is much smaller.

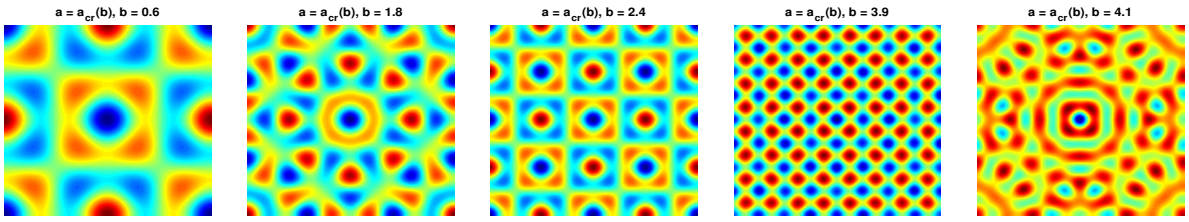

Figure 6: Patterns in the classical Schnakenberg equation with $\kappa_1 = 0.01$.

In Figure 6, we study the patterns at the critical value, i.e., $a = a_{\rm cr}$. It shows that for a given b, patterns start appearing from $a = a_{\rm cr}$, but they are significantly different from those when $a \gg a_{\rm cr}$. Even though the analysis of amplitude equations predicts the existence of spot and stripe patterns, it could not provide the information at the critical values. Hence, numerical studies play an important role in this regime. To the best of our knowledge, no reports of patterns at the critical value $a = a_{\rm cr}$ can be found in the literature.

Next, we move to study the effects of diffusion coefficients κ_1 and κ_2 on pattern selection. Our linear stability analysis suggests that the Turing space depends only on the ratio κ_1/κ_2, and it expands as the ratio decreases. For given parameters a and b, the weakly nonlinear analysis further suggests that the steady patterns remain the same if ratio κ_1/κ_2 is the same. However, do the values of κ_1 and κ_2 play a role on in pattern formation? To understand it, we show the patterns

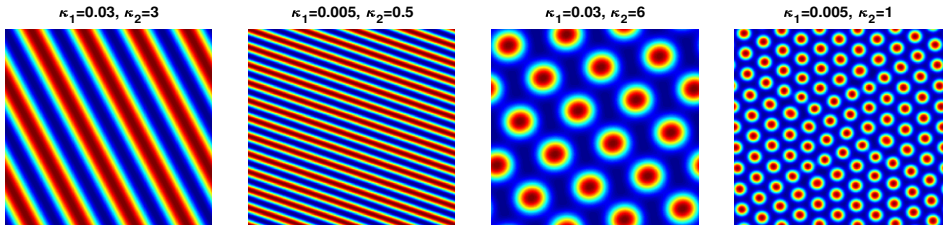

Figure 7: Patterns in the classical Schnakenberg equation with $a = 3.4$ and $b = 3.5$.

for various κ_1 and κ_2 in Figure 7, where $b = 3.5$ and $a = 3.4$. Note that the pattern for $\kappa_1 = 0.01$ and $\kappa_2 = 1$ can be found in Fig. 4 (c). The same initial conditions and numerical parameters are used for Fig. 7 and Fig. 4 (c). For ratio $\kappa_1/\kappa_2 = 0.01$, mixed and stripe patterns are observed in Fig. 4 (c) and Fig. 7, respectively. This might be because $a = 3.4$ and $b = 3.5$ is on the boundary between the stripe region and mixed region (see Fig. 3), and thus a small perturbation can change the steady patterns. As the ratio κ_1/κ_2 decreases, the H_0 spot patterns become more favorable, consistent with our prediction in Fig. 3. On the other hand, the patterns generally remain the same for fixed κ_1/κ_2, but their scales are much smaller with the decrease of product $\kappa_1\kappa_2$, which could be also understood from their dispersion relation in Fig. 8. It shows that for the same diffusion ratio

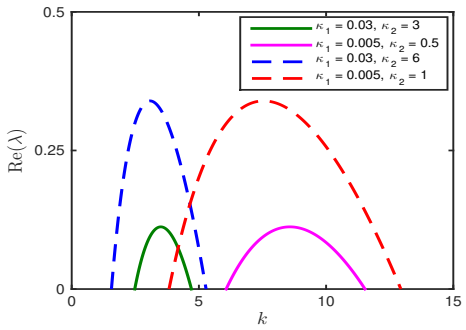

Figure 8: Dispersion relation for patterns in Figure 7.

κ_1/κ_2, the smaller the product $\kappa_1\kappa_2$, the larger the unstable wave numbers, and thus the finer the pattern scales. Hence, the computations of patterns with smaller $\kappa_1\kappa_2$ become more challenging. The above observations suggest the limitations of the linear stability analysis and weakly nonlinear analysis in the study of pattern formations.

5 Pattern formation with superdiffusion

In this section, we study the pattern formation in the Schnakenberg equations when superdiffusion is present in one or both components, i.e., $\gamma_1, \gamma_2 \leq 2$. We will divide our studies into two cases,

i.e., $\gamma_1 = \gamma_2$, and $\gamma_1 \neq \gamma_2$. The effects of superdiffusion on pattern formation will be studied by comparing to the results in Section 4 for the classical Schnakenberg equations.

5.1 Same superdiffusion power $\gamma_1 = \gamma_2$

For simplicity, we denote $\gamma_1 = \gamma_2 = \gamma$. Our linear stability analysis shows that the Turing space in this case is identical to that of the classical Schnakenberg equations. In other words, if $\gamma_1 = \gamma_2$, the diffusion powers play no role in the Turing instability, but they may affect the pattern selections according to our weakly nonlinear analysis. To further our understanding, we compare patterns

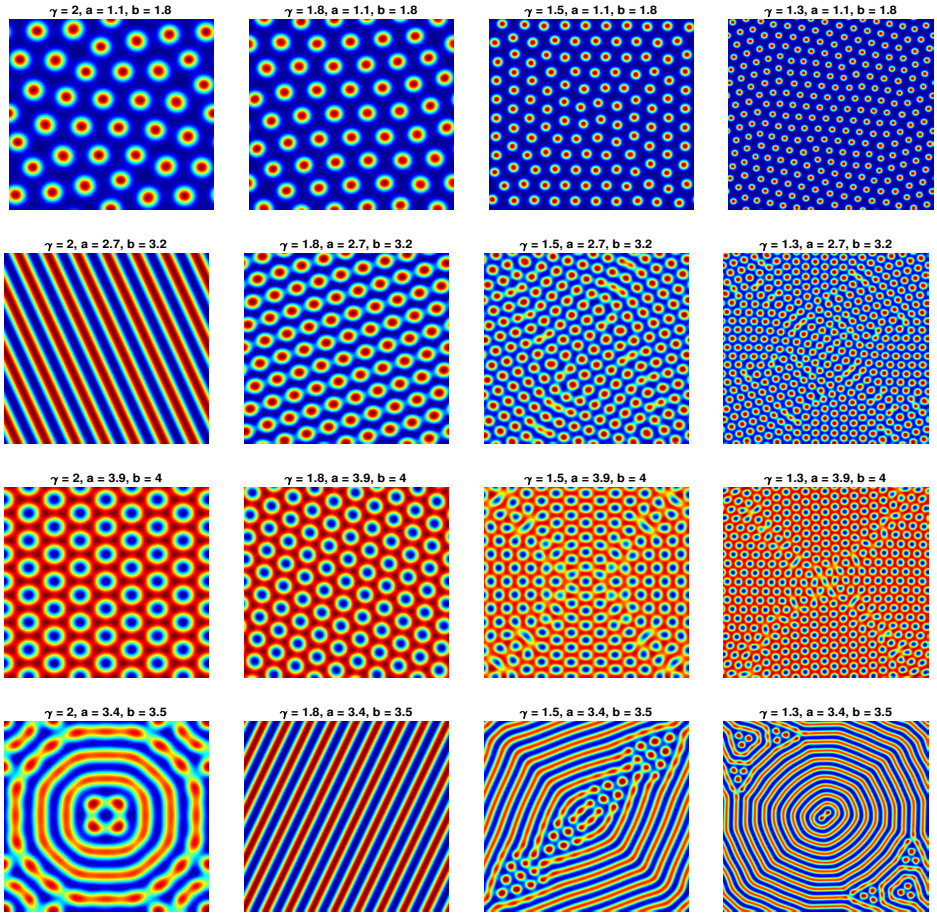

Figure 9: Comparison of patterns in the classical and fractional Schnakenberg equations with $\kappa_1 = 0.01$ and $\kappa_2 = 1$.

in the classical and fractional cases in Figure 9, and when $\gamma = 2$ they are the four representative patterns in Fig. 4. It shows that the patterns in the classical and fractional Schnakenberg equations are qualitatively the same, if a and b are far from the region of mixed patterns (see row 1 and 3 in Fig. 9. However, if a and b are close to or in the region of mixed patterns, the superdiffusion has stronger effects on pattern selection, and a small change of power γ could alter the type of patterns. Generally, the smaller the power γ, the stronger the superdiffusion, the finer the scales of patterns. This can be also indicated in the dispersion relation in Fig. 2 (c) – the smaller the power γ, the larger the unstable wave numbers, implying the finer scales of patterns. Computationally, smaller

mesh size and time step are demanded in order to capture the pattern details in the fractional cases, which greatly increases the computational costs and makes the simulations more challenging.

In Figure 10, we compare the time evolution of the pattern growth in the classical and fractional cases with $a = 2.7$ and $b = 3.2$. The pattern initially emerges as spirals from the center of

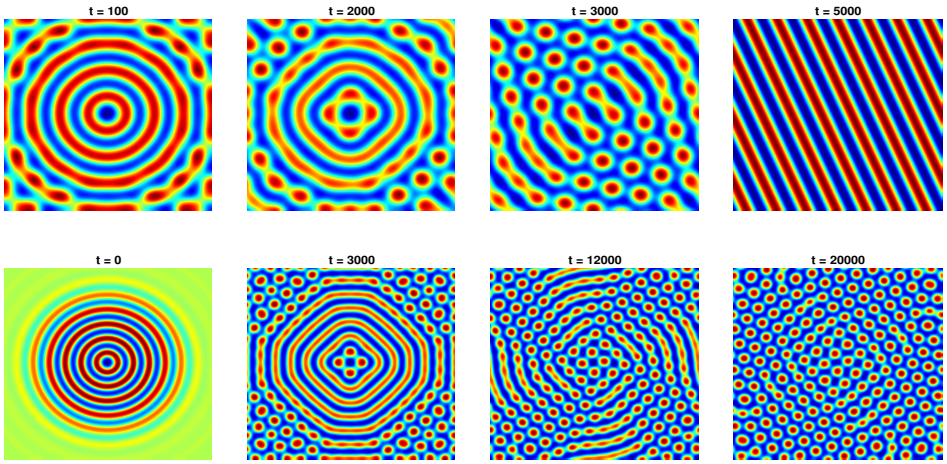

Figure 10: Dynamics of pattern formation in the classical (top row) and fractional (bottom row) Schnakenberg equations with $a = 2.7$ and $b = 3.2$.

perturbation and then radiates towards the boundary. For both classical and fractional cases, the spirals would break into spots once they reach the boundary. Then the spots in the classical cases will reconnect and form into steady stripe patterns, but remain spot patterns in the fractional cases. Moreover, we find that the fractional cases take much longer time to reach the steady patterns. We also study the effects of diffusion coefficients κ_1 and κ_2 on pattern formation and find similar results as in the classical cases. It shows that decreasing either the ratio κ_1/κ_2 or power γ could lead to patterns with smaller scales, but the patterns from decreasing power γ are much denser. For brevity, we will omit showing these patterns here.

5.2 Different superdiffusion power $\gamma_1 \neq \gamma_2$

In the following, we explore the patterns in the fractional Schnakenberg equations when two components have different diffusion powers. We will divide our discussion into two cases: $\gamma_1 < \gamma_2$ and $\gamma_1 > \gamma_2$. Figure 11 compares the Turing spaces of different powers γ_1 and γ_2. As discussed previously, the Turing space increases as the ratio γ_1/γ_2 decreases, and thus the spatially homogenous steady state $\mathbf{u}_s$ is more unstable. The necessary conditions for the Turing instability is $\kappa_1 < \kappa_2$, but the diffusion power γ_1 can be larger than γ_2. Thus, the fractional models introduce more degrees of freedom to start patterns.

Figure 11 shows the patterns for $\gamma_1 < \gamma_2$, where we fix $\gamma_2 = 2$ and $\kappa_1 = 0.01$. It shows that even a small reduction of γ_1 leads to different patterns. For a fixed power γ_2, decreasing γ_1 would expand the Turing space and consequently enlarge the H_0 spot regions. This is confirmed by our results in Fig. 12 – the spot patterns become more favorable as γ_1 decreases. Moreover, the pattern scale reduces with the ratio γ_1/γ_2, as larger unstable wave numbers are presented (see Fig. 2 (b)).

On the other hand, Figure 13 presents the patterns for $\gamma_1 > \gamma_2$, where $\gamma_1 = 2$, $\kappa_1 = 0.01$, and $b = 1.8$ are fixed. For $\gamma_2 = 1.9$, the patterns are located in the H_0 spot regime, and thus similar patterns are observed for all $a_{\text{cr}} < a < b$. With the decrease of γ_2, the Turing space quickly shrinks

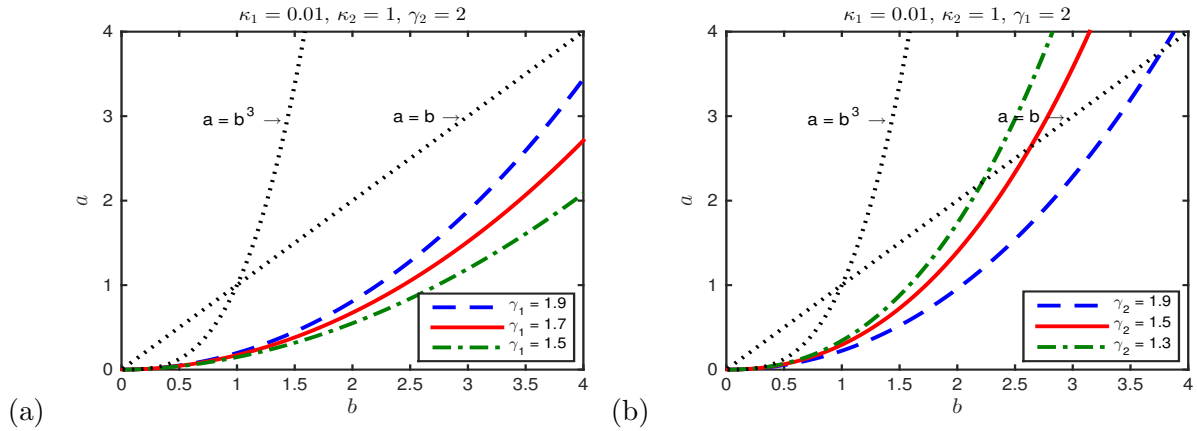

Figure 11: Comparison of Turing spaces (i.e., region between the non-dotted line and dotted-line of $\min\{b, b^3\}$) for different diffusion powers γ_1 and γ_2.

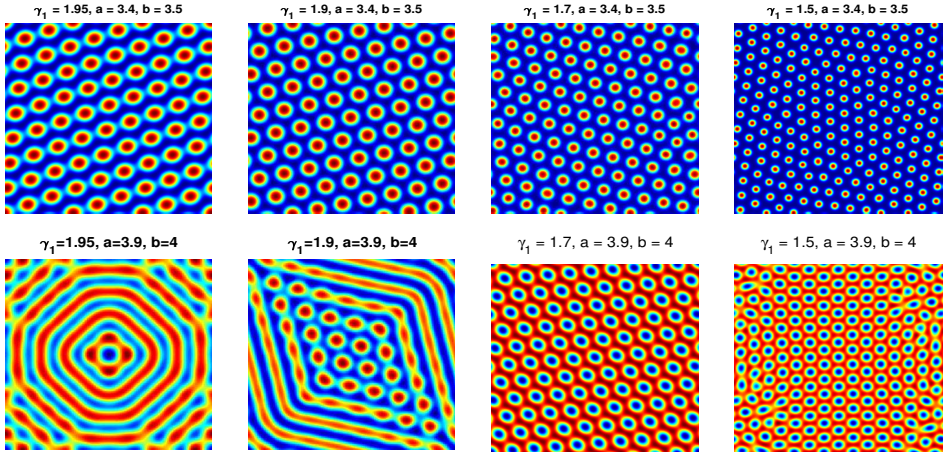

Figure 12: Patterns in the fractional Schnakenberg equations with $\gamma_2 = 2$, $\kappa_1 = 0.01$ and $\kappa_2 = 1$.

(see Fig. 11 (b)), and the parameter $b = 1.8$ is now around the boundary of H_0 spots and mixed pattern regions. Thus different patterns may be observed for different values of a (see Fig. 13 with $\gamma_2 = 1.5$). Note that the dispersion relation of this case is similar to that in Fig. 2 (a).

6 Conclusions

We studied the pattern formation in the classical and fractional Schnakenberg equations and compare the effects of normal and super diffusion on pattern selection. Our studies not only provide a systematic understanding of Turing patterns in the classical Schnakenberg equations but also present detailed comparisons of patterns in classical and fractional models with different parameters. Our linear stability analysis suggested that the Turing space depends on both ratios of κ_1/κ_2 and γ_1/γ_2, which implies that the classical and fractional model with $\gamma_1 = \gamma_2$ have the same Turing space. The Turing space increases as the ratio κ_1/κ_2 or γ_1/γ_2 decreases, and the necessary condition of Turing instability is $\kappa_1 < \kappa_2$. On the other hand, the unstable wave numbers and their growth rates are sensitive to the values of κ_l and γ_l for $l = 1, 2$. Generally, the smaller the

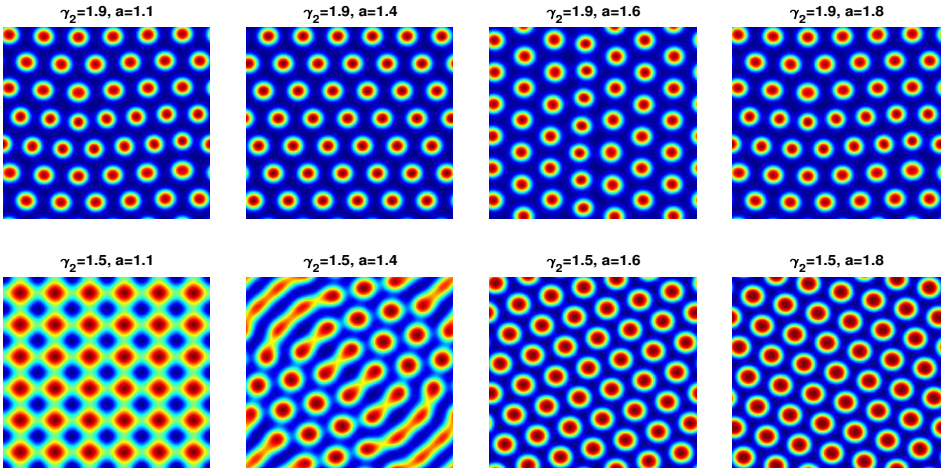

Figure 13: Patterns in the fractional Schnakenberg equation with $\gamma_1 = 2$, $\kappa_1 = 0.01$, $\kappa_2 = 1$, and $b = 1.8$.

power γ_1, the larger the unstable wave numbers and the smaller the pattern scales. Our weakly nonlinear analysis predicted the parameter regimes where hexagons, stripes, and their coexistence are expected in the Turing space. We numerically explored the interactions of diffusion coefficients and diffusion powers on the emergence of Turing patterns. Our numerical results confirmed the theoretical analysis and also provided new insights on the patterns in the fractional Schnakenberg equations.

Acknowledgements. This work was supported by the US National Science Foundation under Grant Number DMS-1620465.

References

[1] Aragon, J.L., Varea, C., Barrio, R.A., Maini, P.K.: Spatial patterning in modified Turing systems: Application to pigmentation patterns on marine fish. Froma **13**, 145–254 (1998)

[2] Barrio, R.A., Baker, R.E., Vaughan, B., Tribuzy, K., de Carvalho, M.R., Bassanezi, R., Maini, P.K.: Modeling the skin pattern of fishes. Phys. Rev. E **79**, 031908 (2009)

[3] Beentjes, C.H.: Pattern formation analysis in the Schnakenberg model. Technical Report, University of Oxford, UK (2015)

[4] Bueno-Orovio, A., Kay, D., Burrage, K.: Fourier spectral methods for fractional-in-space reaction-diffusion equations. BIT **54**, 937–954 (2014)

[5] del Castillo-Negrete, D., Carreras, B.A., Lynch, V.E.: Front dynamics in reaction-diffusion systems with Lévy flights: A fractional diffusion approach. Phys. Rev. Lett. **91**, 018302 (2003)

[6] Cusimano, N., Bueno-Orovio, A., Turner, I., Burrage, K.: On the order of the fractional Laplacian in determining the spatio-temporal evolution of a space-fractional model of cardiac electrophysiology. Plos One **10**, e0143938 (2015)

[7] Duo, S., Zhang, Y.: Mass conservative method for solving the fractional nonlinear Schrödinger equation. Comput. Math. Appl. **71**, 2257–2271 (2016)

[8] Dutt, A.K.: Amplitude equation for a diffusion-reaction system: The reversible Sel'kov model. AIP. Advances **2**, 042125 (2012)

[9] Gafiychuk, V.V., Datsko, B.Y.: Spatiotemporal pattern formation in fractional reaction-diffusion systems with indices of different order. Phys. Rev. E **77**, 066210 (2008)

[10] Gafiychuk, V.V., Datsko, B.Y.: Mathematical modeling of different types of instabilities in time fractional reaction-diffusion systems. J. Comput. Appl. Math. **59**, 1101–1107 (2010)

[11] Garvie, M.R., Burkardt, J., Morgan, J.: Simple finite element methods for approximating predator-prey dynamics in two dimensions using Matlab. Bull. Math. Biol. **77**(3), 548–578 (2015)

[12] Giona, M., Cerblli, S., Roman, H.E.: Fractional diffusion equation and relaxation in complex viscoelastic materials. Physica A **191**, 449–453 (1992)

[13] Golovin, A.A., Matkowsky, B.J., Volpert, V.A.: Turing pattern formation in the Brusselator model with superdiffusion. SIAM. J. Appl. Dyn. Syst. **69**, 251–272 (2008)

[14] Gomez, D., Mei, L., Wei, J.: Stable and unstable periodic spiky solutions for the Gray–Scott system and the Schnakenberg system. J. Dyn. Differ. Equ. **32**, 441–481 (2020)

[15] Hammouch, Z., Mekkaoui, T., Belgacem, F.B.M.: Numerical simulations for a variable order fractional Schnakenberg model. AIP. Conf. Proc. **1637**, 1450–1455 (2014)

[16] Hao, W., Xue, C.: Spatial pattern formation in reaction-diffusion models: A computational approach. J. Math. Biol. **80**(1–2), 521–543 (2020)

[17] Hofling, F., Franosch, T.: Anomalous transport in the crowded world of biological cells. Rep. Prog. Phys. **76**, 046602 (2013)

[18] Hornung, G., Berkowitz, B., Barkai, N.: Morphogen gradient formation in a complex environment: An anomalous diffusion model. Phys. Rev. E **72**, 041916 (2005)

[19] Iron, D., Wei, J., Winter, M.: Stability analysis of Turing patterns generated by the Schnakenberg model. J. Math. Biol. **49**, 358–390 (2004)

[20] Kirkpatrick, K., Zhang, Y.: Fractional Schrödinger dynamics and decoherence. Physica D **332**, 41–54 (2016)

[21] Kolokolnikov, T., Ward, M.J., J., W.: Spot self-replication and dynamics for the Schnakenberg model in a two-dimensional domain. J. Nonlinear Sci. **19**, 1–56 (2009)

[22] Li, B., Zhang, X.: Steady states of a Sel'kov–Schnakenberg reaction-diffusion system. Discret Contin. Dyn. S. **10**, 1009–1023 (2017)

[23] Li, Y.: Steady-state solution for a general Schnakenberg model. Nonlinear Anal-Real. **12**, 1985–1990 (2011)

[24] Li, Y., Jiang, J.: Pattern formation of a Schnakenberg-type plant root hair initiation model. Electron J. Qual. Theo. **88**, 1–19 (2018)

[25] Liu, G., Wang, Y.: Pattern formation of a coupled two-cell Schnakenberg model. Discret Contin. Dyn. S **10**, 1051–1062 (2017)

[26] Liu, P., Shi, J., Wang, Y., Feng, X.: Bifurcation analysis of reaction-diffusion Schnakenberg model. J. Math. Chem. **51**, 2001–2019 (2013)

[27] Metzler, R., Klafter, J.: The random walk's guide to anomalous diffusion: A fractional dynamics approach. Phys. Rep. **339**, 1–77 (2000)

[28] Naether, U., Stutzer, S., Vicencio, R.A., Molina, M.I., Tunnermann, A., Nolte, S., Kottos, T., N., C.D., Szameit, A.: Experimental observation of superdiffusive transport in random dimer lattices. New J. Phys. **13**, 013045 (2013)

[29] Prytula, Z.: Amplitude equations for activator-inhibitor system with superdiffusion. Math. Mod. Comput. **3**, 191–198 (2016)

[30] Ren F.Y., Liang, J.R., Qiu, W.Y., Wang, X.T., Xua, Y., Nigmatullin, R.R.: An anomalous diffusion model in an external force fields on fractals. Phys. Lett. **312**, 187–197 (2003)

[31] Schnakenberg, J.: Simple chemical reaction systems with limit cycle behaviour. J. Theor. Biol. **81**, 389–400 (1979)

[32] Shaw, L.J., Murray, D.: Analysis of a model for complex skin patterns. SIAM J. Appl. Dyn. Syst. **50**, 628–648 (1990)

[33] Shlesinger, M.F., West, B.J., Klafter, J.: Lévy dynamics of enhanced diffusion: Application to turbulence. Phys. Rev. Letts. **58**, 1100–1103 (1987)

[34] Ward, M.J., Wei, J.: The existence and stability of asymmetric spike patterns for the Schnakenberg model. Stud. Appl. Math. **109**, 229–264 (2002)

[35] Wei, J., Winter, M.: Flow-distributed spikes for Schnakenberg kinetics. J. Math. Biol **64**, 211–254 (2012)

[36] Wu, J., Wu, X.: Bogdanov-Takens singularity for a system of reaction-diffusion equations. J. Math. Chem. **54**(1), 120–136 (2016)

[37] Xu, C., Wei, J.: Hopf bifurcation analysis in a one-dimensional Schnakenberg reaction-diffusion model. Nonlinear Anal-Real. **13**, 1961–1977 (2012)

[38] Yi, F., Gaffney, E.A., Lee, S.S.: The bifurcation analysis of Turing pattern formation induced by delay and diffusion in the Schnakenberg system. Discret Contin. Dyn. B. **22**, 647–668 (2017)

[39] Zhang, L., Tian, C.: Turing pattern dynamics in an activator-inhibitor system with superdiffusion. Phys. Rev. E. **90**, 062915 (2014)

[40] Zimbardo, G., Amato, E., Bovet, A., Effenberger, F., Fasoli, A., Fichtner, H., Furno, I., Gustafson, K., Ricci, P., Perri, S.: Superdiffusive transport in laboratory and astrophysical plasmas. J. Plasma Phys. **81**, 495810601 (2015)